

LDV Measurement, Flow Visualization and Numerical Analysis of Flow Distribution in a Close-Coupled Catalytic Converter

Duk-Sang Kim*

Graduate School of Automotive Engineering, Kookmin University, Seoul 136-702, Korea

Yong-Seok Cho

Graduate School of Automotive Engineering, Kookmin University, Seoul 136-702, Korea

Results from an experimental study of flow distribution in a close-coupled catalytic converter (CCC) are presented. The experiments were carried out with a flow measurement system specially designed for this study under steady and transient flow conditions. A pitot tube was a tool for measuring flow distribution at the exit of the first monolith. The flow distribution of the CCC was also measured by LDV system and flow visualization. Results from numerical analysis are also presented. Experimental results showed that the flow uniformity index decreases as flow Reynolds number increases. In steady flow conditions, the flow through each exhaust pipe made some flow concentrations on a specific region of the CCC inlet. The transient test results showed that the flow through each exhaust pipe in the engine firing order, interacted with each other to ensure that the flow distribution was uniform. The results of numerical analysis were qualitatively accepted with experimental results. They supported and helped explain the flow in the entry region of CCC.

Key Words : Close-coupled Catalytic Converter, Exhaust Gas After-Treatment, Exhaust Gas Flow Distribution, Flow Visualization, LDV (Laser Doffler Velocimetry), Numerical Analysis

Nomenclature

C_μ : Turbulent dissipation coefficient
 I : Turbulent intensity
 K : Permeability coefficient
 k : Turbulent energy
 P : Pressure
 T : Temperature
 U : Velocity vector component
 u : Turbulent fluctuation velocity component
 V : Velocity at the monolith
 X : Cartesian coordinate component
 α, β : Permeability coefficient factor
 δ : Kronecker's delta
 ϵ : Turbulent dissipation

μ : Viscosity

ρ : Density

1. Introduction

Recently, the after-treatment of the automotive engine emission is increasingly important for the reduction of pollutant materials, which cause the environmental disruption. Several studies have been performed to solve the emission problem for various engines including CNG, diesel and LPG. (Min et al., 2002; Choi et al., 2003; Kim and Min, 2001) Specifically, the three-way catalyst for gasoline engine is at the center of these studies. The three-way catalytic converter, which is widely used in passenger cars today, is one of the most effective devices for exhaust gas after-treatment. However, it requires some warm-up period during the cold start to reach the light-off temperature above which the conversion efficiency

* Corresponding Author,

E-mail : lordduke@kookmin.ac.kr

TEL : +82-2-910-5027; FAX : +82-2-942-7721

Graduate School of Automotive Engineering, Kookmin University, Seoul 136-702, Korea. (Manuscript Received October 18, 2003; Revised July 30, 2004)

becomes sufficiently high. During this warm-up period, the conversion efficiency is very low and the maximum portion of unburned HC is emitted.

Close-coupled Catalytic Converter (CCC) is one of the efforts to reduce the initial emissions during the cold start. The catalytic converter is mounted close to the exhaust manifold to use the exhaust gas heat with as little loss as possible, and to raise the converter temperature quickly. This method is cost-effective and efficient. However, the lack of flow uniformity causes lower conversion efficiency and reduces the catalyst's reliability. It is generally understood that uniform flow distribution at the catalyst improves the conversion efficiency and durability of the catalytic converter. Uniform flow distribution at the monolith inlet lowers local peak velocity and temperature gradient in the catalytic converter, and delays wear-out of the catalytic converter (Cho et al., 2001 ; Kim et al., 1992). It will be possible that a reduced-volume CCC can have the same durability if the flow distribution becomes uniform. This leads to a reduction in cost and mass of the CCC (Cho et al., 2001).

The key factor in designing a CCC is to match the geometry and position between exhaust manifold and CCC. If they are poorly designed, flow at the monolith inlet becomes highly irregular, resulting in poor catalyst conversion efficiency and durability. Therefore, the design of exhaust manifold, inducing exhaust flow uniformity that means uniform velocity distribution of exhaust gas at the face of catalytic monolith, is essential for the implementation.

In this study, the pitot tube and LDV (Laser Doffler Velocimetry) measured the exhaust flow distribution in the engine simulation device at the entrance of CCC, and numerical analysis was also performed using STAR-CD, which is a commercial CFD (Computational Fluid Dynamics) code for the optimum design of exhaust system.

2. Experimental Apparatus

Due to the difficulties of optical approach in

the real operating engine, a flow simulation device was designed for measurements. As shown in Fig. 1, this apparatus can simulate the exhaust flow of engine by supplying the room temperature air with roots blower. The airflow rate is controlled through the orifice and a bypass valve. The blower supplies air through the exhaust manifold and the CCC. The maximum flow rate is $7 \text{ m}^3/\text{min}$, which is enough to simulate the full load condition at 6000 rpm of a 1.5 liter engine. Analogy of Reynolds numbers is applied between hot exhaust gas and cold room temperature air to determine the experimental conditions of the system. The changes of temperature and gas components in the measurement system lead to the change of Reynolds number when the flow rate of the system is same with the engine and thus turbulence characteristics. Therefore the flow rate of the system is controlled to have same Reynolds number with the real engine. The measurement was taken under two airflow conditions. One is the steady flow condition in which the air flows through only one manifold branch and the other is the transient condition in which air flows sequentially through all the branches, as in the real engine. The rotary valve unit, which can simulate the flow characteristics of valve overlap, controlled this sequential flow.

The experiment was carried out under flow rate conditions of 2500 and 4000 rpm. In the steady flow condition, the measurement was carried out when valve 1 or valve 2 was open. Under the transient condition, all the valves were sequentially operated, as above mentioned.

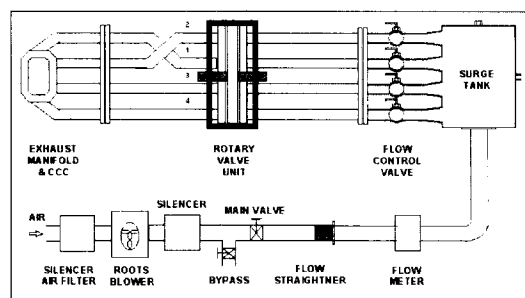


Fig. 1 CCC flow measurement system and flow distribution measurement using a pitot tube

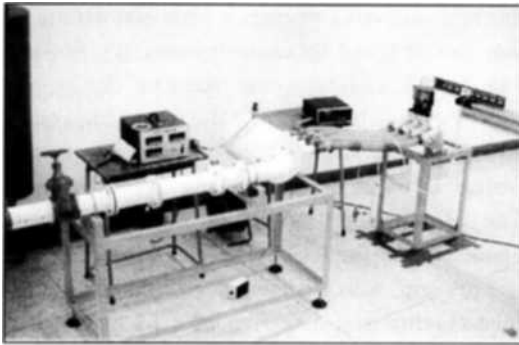


Fig. 2 CCC flow measurement system and flow distribution measurement using a pitot tube

2.1 Flow distribution measurement using pitot tube

The monolith in the CCC is a ceramic block that has many narrow channels. It is reasonable to assume that the flow entered in each channel does not interfere with the flow in adjacent channels, and that the flow distribution at the monolith inlet is the same as the flow distribution at the exit of the first monolith. Based on this assumption, the velocity profiles are measured at the exit of the first monolith using a pitot tube. The pitot tube has the fixed measuring point and is moved by a 3-axis traverse for precise measurements, from Fig. 2.

2.2 Flow distribution measurement using LDV

Fig. 3 represents the LDV system of this study. LDV measures velocity of a particle that passes through the measuring point. The point is generated by cross section of two laser beams. The particle emits Doppler burst signal by virtue of the frequency difference between beams. This system consists of Ar-ion laser source, fiber drive, transmitting optics including Bragg cells, receiving optics, RSA (Real-time Signal Analyzer) and DFT (Discrete Fourier Transform). The laser of 2 W output power was operated in double beam mode at 514.5 and 488 nm to measure 2-dimensional velocity distributions.

2.3 Flow visualization

The flow field was visualized by the Mie scat-

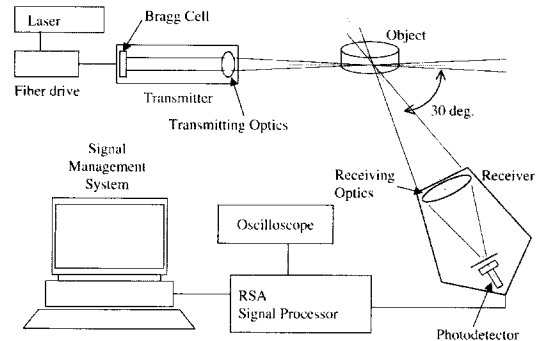


Fig. 3 Schematic Diagram of LDV system

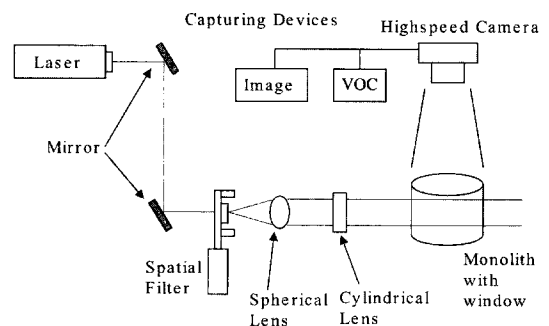


Fig. 4 Schematic diagram of flow visualization

tering method by mixing the particles into the airflow and applying a sheet laser beam to the test section. The images were captured by a high speed Kodak Memrecam Ci camera. To eliminate the intensity drift due to floating particles in the air, a spatial filter was mounted to maintain the intensity of the beam. A particle seeder of fluidized-bead type was used for uniform particle concentration. The seeding particle was titanium-dioxide (TiO_2). Fig. 4 shows the schematics of this system.

3. Numerical Analysis of Flow Distribution

3.1 Governing equations

In the numerical analysis of flow distribution, standard $k-\epsilon$ model was used for turbulent flow and the governing equations are as follows (Star-CD Ver. 3.0 User's Manual, 1996):

Continuity equation :

$$\frac{\partial(\rho U_i)}{\partial x_i} = 0 \tag{1}$$

Navier-Stokes equation in turbulent momentum :

$$\begin{aligned} \frac{\partial(\rho U_i)}{\partial t} + U_j \frac{\partial(\rho U_i)}{\partial x_j} \\ = -\frac{\partial P}{\partial x_i} + \frac{\partial}{\partial x_j} \left(\mu \frac{\partial U_i}{\partial x_j} - \overline{\rho u_i u_j} \right) \end{aligned} \tag{2}$$

Turbulence model is given as

$$\overline{\rho u_i u_j} = \mu_t \left(\frac{\partial U_i}{\partial x_j} + \frac{\partial U_j}{\partial x_i} \right) - \frac{2}{3} \rho k \delta_{ij} \tag{3}$$

where the turbulent viscosity is $\mu_t = \frac{C_\mu \rho k^2}{\epsilon}$

Transport equations for the standard $k-\epsilon$ model are

$$\begin{aligned} \frac{\partial(\rho k)}{\partial t} + \frac{\partial(\rho U_i k)}{\partial x_i} \\ = \rho P - \rho \epsilon + \frac{\partial}{\partial x_i} \left[\left(\mu + \frac{\mu_t}{\sigma_k} \right) \frac{\partial k}{\partial x_i} \right] \end{aligned} \tag{4}$$

$$\begin{aligned} \frac{\partial(\rho \epsilon)}{\partial t} + \frac{\partial(\rho U_i \epsilon)}{\partial x_i} \\ = C_{\epsilon_1} \frac{\rho P \epsilon}{k} - C_{\epsilon_2} \frac{\rho \epsilon^2}{k} + \frac{\partial}{\partial x_i} \left[\left(\mu + \frac{\mu_t}{\sigma_\epsilon} \right) \frac{\partial \epsilon}{\partial x_i} \right] \end{aligned} \tag{5}$$

where the production term P is defined as

$$P = \frac{\mu_t}{\rho} \left(\frac{\partial U_i}{\partial x_j} + \frac{\partial U_j}{\partial x_i} - \frac{2}{3} \frac{\partial U_m}{\partial x_m} \delta_{ij} \right) \frac{\partial U_i}{\partial x_j} - \frac{2}{3} k \frac{\partial U_m}{\partial x_m} \tag{6}$$

Boundary conditions for standard $k-\epsilon$ model are given as

$$k = 1.5 (I \times U)^2, \quad \epsilon = \frac{C_\mu^{0.75} k^{1.5}}{L} \tag{7}$$

where I is the turbulence intensity, C_μ is the turbulence coefficient and L is the characteristic length. Five constants determined for this study are (Lai et al., 1991);

$$C_\mu = 0.09, \quad C_{\epsilon_1} = 1.44, \quad C_{\epsilon_2} = 1.92, \quad \sigma_k = 1.0, \quad \sigma_\epsilon = 1.3$$

The wall theory was applied to avoid grid point concentration due to stiff velocity gradient. Simple algorithm and upwind scheme were applied to solve the velocity terms of the above equations. Fig. 5 represents 3-D modeling of the manifold and CCC shape in this analysis. In the numerical analysis, the airflow was assumed to be

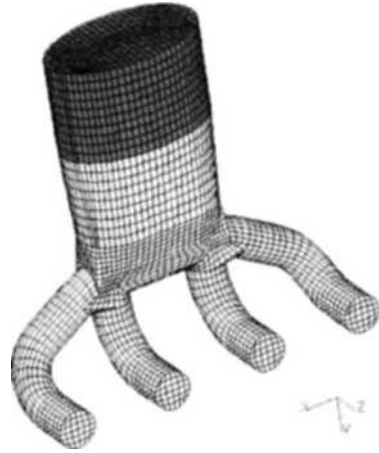


Fig. 5 3-D model of CCC inlet and exhaust manifold

incompressible. The velocity at the inlet of manifold was used as the initial conditions of steady flow and the velocity at the CCC inlet was used for those of the transient flow. The initial conditions for transient flow were varied as 72 steps to compare the result with the experimental data.

3.1.1 Porous material

As the substrate of catalyst is composed of small ceramic flow path, the flow characteristics and the characteristics of flow through the substrate were numerically analyzed under the assumption of porous media. This media plays a pressure resistance in the substrate flow and the pressure drop is expressed as following equation.

$$\frac{\partial P}{\partial x_i} = -K_i u_i, \quad K_i = \alpha_i |\vec{V}| + \beta_i \tag{8}$$

K_i : Permeability Coefficient

In this study, α, β were obtained by regression analysis of pressure drop characteristic curve, which was the result of reference experiments (Kim et al., 1992 ; Lai et al., 1991).

4. Results and Discussion

In the study, uniformity index is defined and applied to evaluate how much the flow is distributed uniformly. The index integrates the difference between local velocity at the measuring point

and the mean velocity of a test. When the flow has uniform distribution, the index goes to unity (Weltens et al., 1993).

$$\gamma = 1 - \frac{1}{2n} \sum_{i=1}^n \frac{\sqrt{(u_i - \bar{u})^2}}{\bar{u}} \quad (9)$$

4.1 Steady flow — at the end of the first monolith

A real engine will always run under unsteady operating conditions. However, the steady flow tests supports important information of design quality such as flow concentration of the CCC monolith.

Figure 6 shows velocity profiles at the monolith with the pipe 1 open at 2500 and 4000 rpm, under steady condition. Reynolds numbers are 9400 for

2500 rpm, and 14800 for 4000, respectively. Mean flow velocities at the monolith are 1.55 and 2.43 m/s, respectively. It is observed that the flow from the pipe 1 concentrates under the pipe 4 because the pipe 1 is inclined at that direction. Also, higher velocity areas are found on the far side from the engine due to inertial effect induced by the pipe bend. In general, velocity close to the wall is higher than monolith center velocity. This makes the velocity profile un-symmetric, like a skewed crater. It is supposed that the pipe bend and inclination create inertial effects causing an inclined tumble and a swirl flow along the inside wall of the plenum and CCC inlet.

The velocity profiles for the two cases are similar, but the flow concentration is stronger in

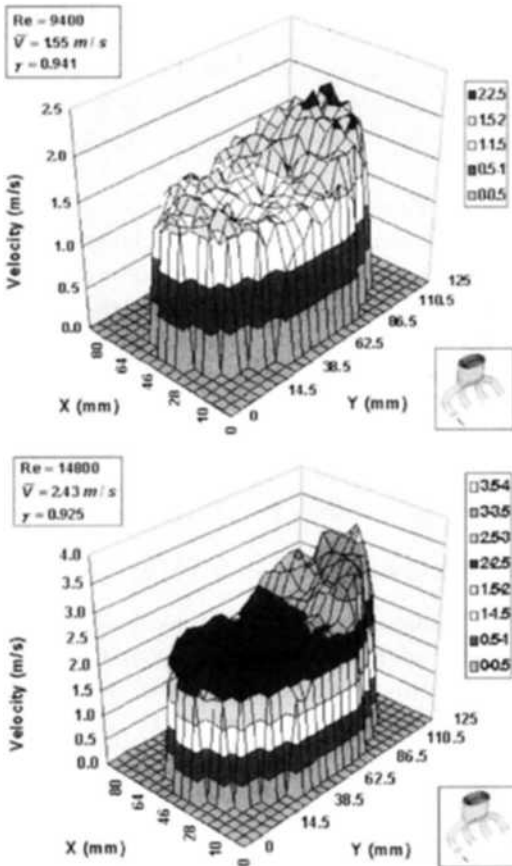


Fig. 6 Velocity profiles for steady flow test conditions with the pipe 1 open at 2500 rpm (top) and 4000 rpm (bottom)

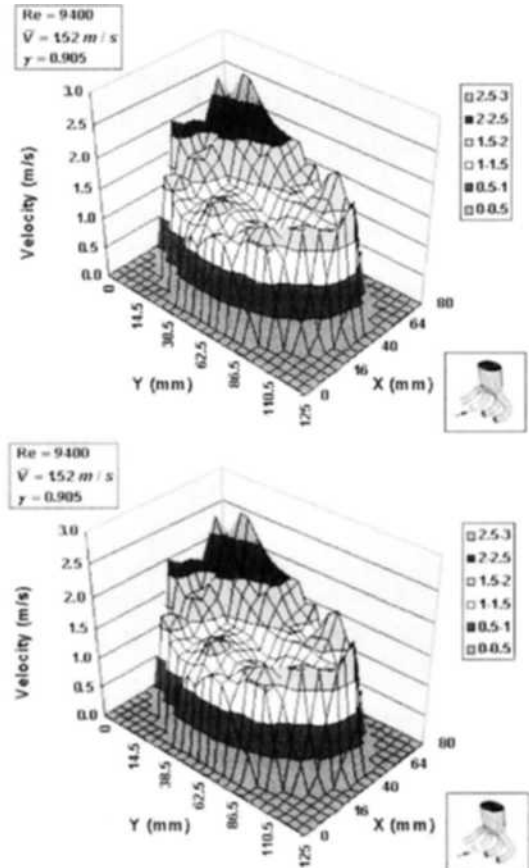


Fig. 7 Velocity profiles for steady flow test conditions with the pipe 2 open at 2500 rpm (top) and 4000 rpm (bottom)

the 4000 rpm case. Difference between the peak and minimum velocities is larger so the un-symmetric profile becomes stronger than 2500 rpm case. Increased inertial force of the flow is considered to be responsible for these phenomena. Thus it can be said that the flow distribution under steady flow conditions is getting worse as the flow rate increases. The uniformity indices of the two cases are 0.941 at 2500 rpm and 0.925 at 4000 rpm.

Figure 7 shows the velocity profiles at the monolith for steady flow conditions with the pipe 2 open at 2500 and 4000 rpm. The pipe 2 merges to the plenum at a right angle, and therefore the flow concentration occurs mainly downstream of the pipe 2. The higher velocity area is found on the farther side from the engine due to the pipe

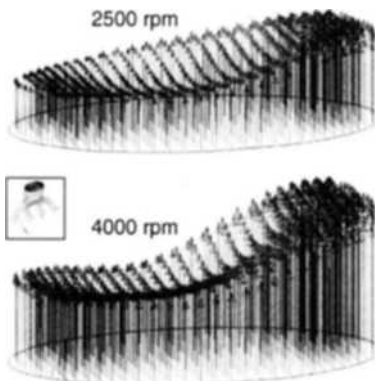


Fig. 8 Velocity vector plots from steady flow calculation with pipe 1 open at 2500 and 4000 rpm

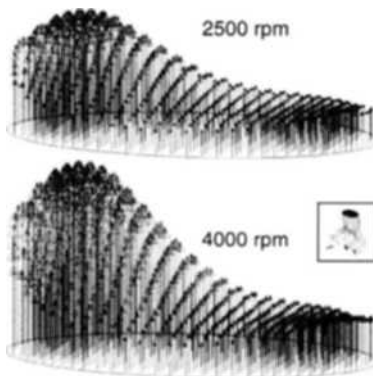


Fig. 9 Velocity vector plots from steady flow calculation with pipe 2 open at 2500 and 4000 rpm

curvature. Flow concentration of the pipe 2 is stronger than that of the pipe 1, due to the short travel length from the exit to monolith surface. The uniformity indices are 0.905 and 0.895 for 2500 and 4000 rpm, respectively.

Figures 8 and 9 show the velocity vector obtained by CFD analysis under steady flow condition. Qualitatively, the analysis results agree with the measurements very well. However, for the case of pipe 2 open, the velocity in the center region are not lower than those of the outer region, showing a little discrepancy from the experimental results given in Fig. 7. The uniformity indices are 0.88 and 0.79 for 2500 and 4000 rpm with the pipe 1 open, respectively, and 0.87 and 0.76 with the pipe 2 open. It is considered that a careful choice of the pressure drop coefficients α and β is needed to obtain more accurate result in the analysis. Nevertheless, the tendency, of which the uniformity index is higher for the pipe 1 open case and the uniformity index decreases as the Reynolds number increases, can be predicted and effectively used when designing a CCC system.

4.2 Steady flow — at the entrance of the first monolith

To measure the velocity distribution at the entrance of the first monolith, the LDV and high speed imaging methods are applied.

Figure 10 shows the results of the LDV measurement and numerical analysis in flow measurement system when valve 1 is open. It is found that the flow concentrates on the opposite side of CCC inlet and a large-scale swirl is formed in the downstream. The reason of this phenomenon is due to the fact that the exhaust pipe is bent and inclined. These phenomena are observed more clearly in the high speed imaging result. Fig. 11 shows one of a high-speed imaging. In this figure, it is also observed that the flow concentrates on a part away from the branch and a large-scale swirl motion is formed beneath the branch. The numerical analysis result, shown in Fig. 12, also shows the concentration.

The results of the experiment and the analysis of branch 2 is shown in Fig. 13 and the high speed image at 2500 rpm is also shown in Fig 14.

In this case, the flow concentration on the downstream of branch is observed and a large-scale swirl is formed on the opposite side.

The section vector plots for steady flow conditions, when the pipe 1 and 2 are open at 2500 rpm, are presented in Fig. 12 and 15. They coincide with the experimental results. The flow exiting the pipe 1 arrives at the opposite wall on the pipe 4 side and re-circulates to the pipe 1 side, yielding

an inclined tumble and swirl. This shows clearly why the flow concentrates below the pipe 4. On the other hand, the flow from the pipe 2 mainly concentrates directly downstream and a weak re-circulation zone is formed below the pipe 4, supporting the experimental results. This clearly shows that the location of flow concentration greatly depends on the configuration of the exhaust manifold.

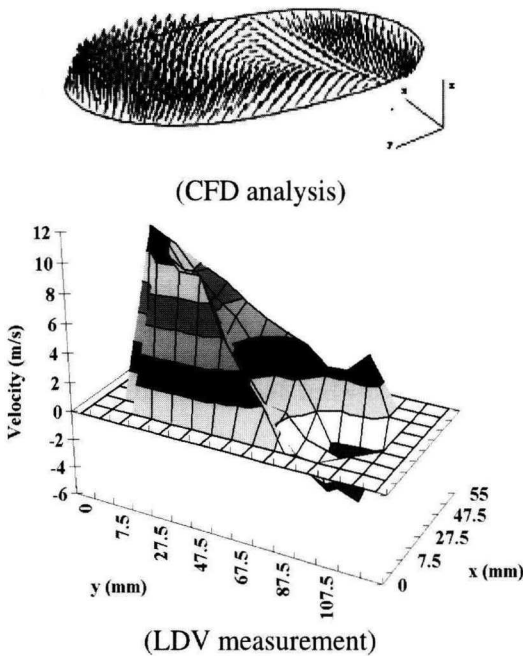


Fig. 10 Comparison between LDV measurement and numerical analysis in steady flow, 2500 rpm, valve 1 open condition

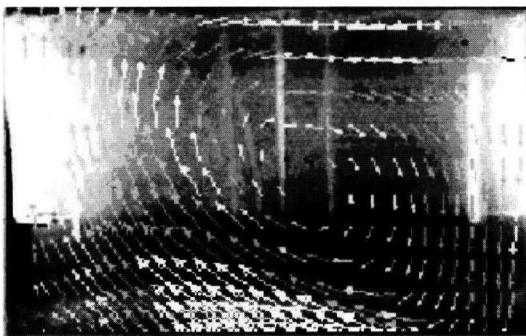


Fig. 11 Flow visualization in steady flow, 2500 rpm, valve 1 open condition

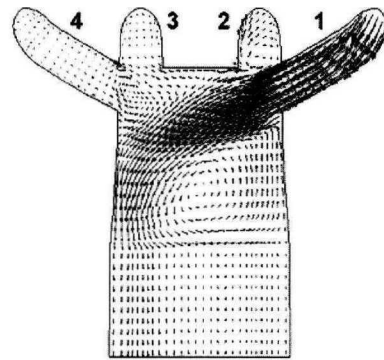


Fig. 12 Section vector plots from steady flow calculation, 2500 rpm, valve 1 open condition

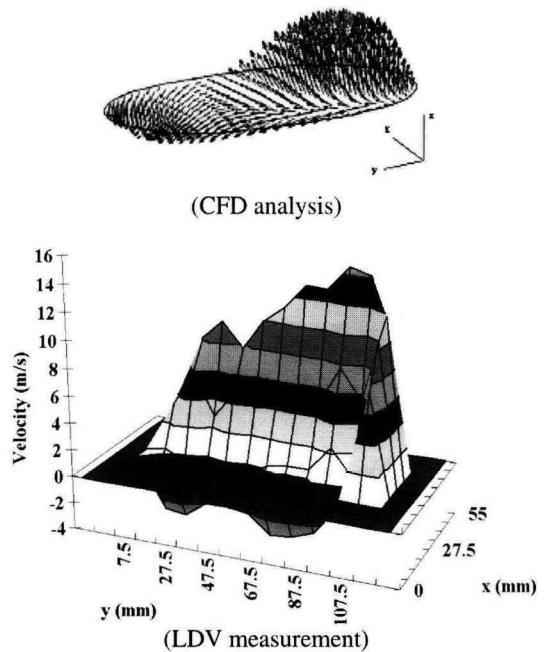


Fig. 13 Comparison between LDV measurement and numerical analysis in steady flow, 2500 rpm, valve 2 open conditions

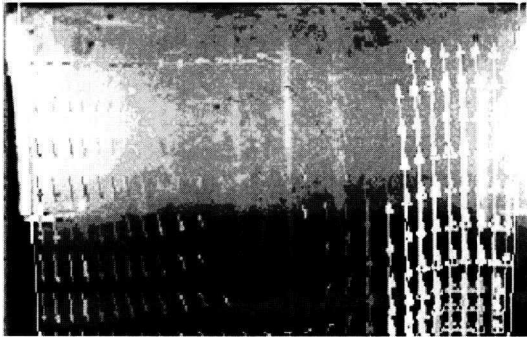


Fig. 14 Flow visualization in steady flow, 2500 rpm, valve 2 open conditions

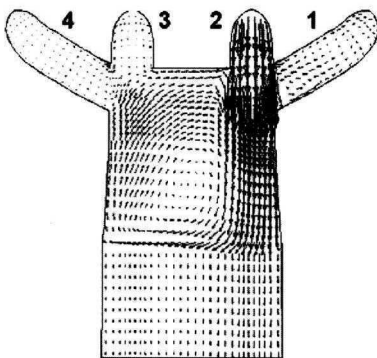


Fig. 15 Section vector plots from steady flow calculation with pipe 1 (top) and pipe 2 (bottom) open at 2500 rpm

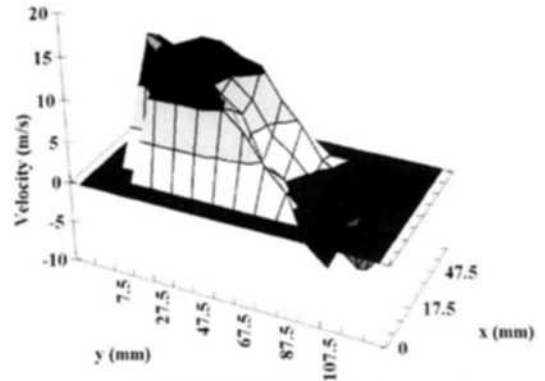
4.3 Transient flow

Transient test results are given in Fig. 18 where velocity profiles at 2500 and 4000 rpm are shown. The shape of the velocity profile looks like a skewed crater, which is symmetrical to the short axes of the monolith, validating symmetrical design of the exhaust manifold. Flow concentration on the far side of the monolith shows inertial effect due to the pipe bends. Higher velocity area along the inside wall results from the inclined tumble and swirl from the pipes 1 and 4. The uniformity indices of the transient flow conditions are 0.943 at 2500 rpm and 0.930 at 4000 rpm. Similarly, according to the steady test, the higher the engine speed, the lower is the uniformity index. It is considered that the increased inertial force at a higher flow rate leads to the result.

The transient flow yields a higher uniformity

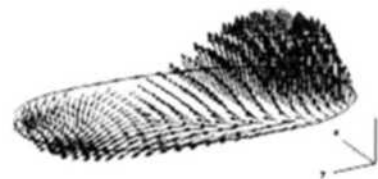


(CFD analysis)

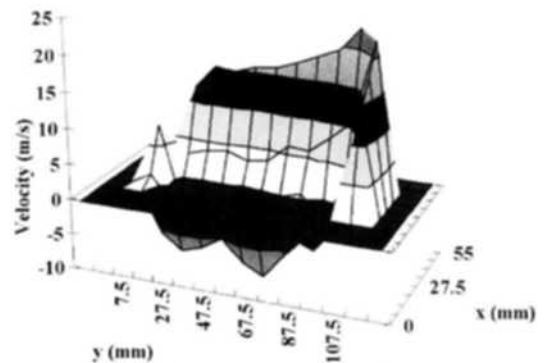


(LDV measurement)

Fig. 16 Comparison between LDV measurement and numerical analysis in steady flow, 4000 rpm, valve 1 open condition



(CFD analysis)



(LDV measurement)

Fig. 17 Comparison between LDV measurement and numerical analysis in steady flow, 4000 rpm, valve 2 open condition

index than steady flow because the flow through each pipe interacts with each other, in a manner so as to expand the flow more quickly and uniformly. It is also observed that the velocity of near the wall or outer flow is faster than that of the center due to the bend and incline of the pipe. Especially, the velocity increase as is far from the engine. Numerical analysis will support this argument later.

Figure 19 represents the experimental result of transient flow using LDV. This shows that air-flow is more uniform than that of steady case due to the interference of each branch flow, similarly with the previous description.

Under transient conditions, the exhaust gas

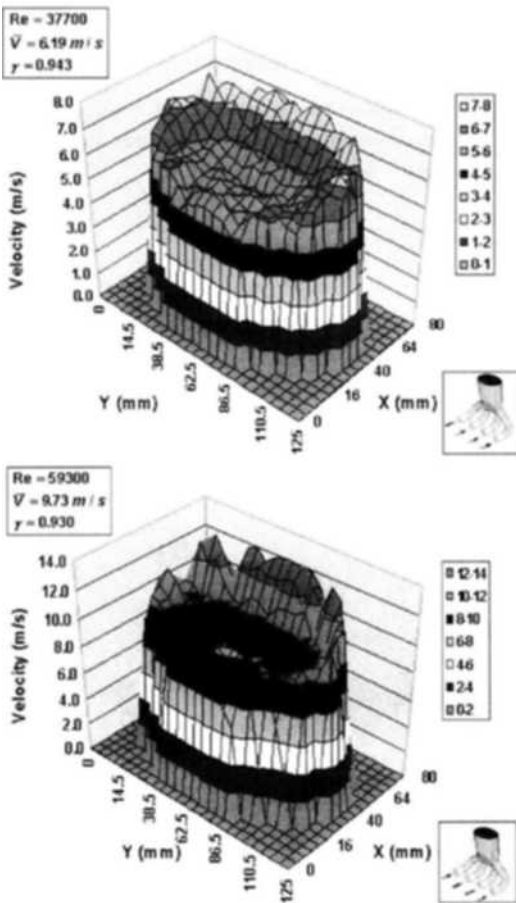


Fig. 18 Velocity profiles for transient flow test conditions at 2500 rpm (top) and 4000 rpm (bottom)

flows through each pipe in the engine firing order (1-3-4-2) as shown in Fig. 20. The mean flow velocity through each pipe is 10 m/s, and the computation has been performed for every 2° crank angle (CA). Fig. 20 shows the representative sequences of the flow in the CCC under the transient flow condition. The vector plots, A to D, represent the velocity vector fields at 60° CA after the flow entry at each pipe, and the interval between each plot is 180° CA.

As shown in these plots the flow fields formed by the earlier and later exhaust, interact with each other in the CCC. For example, the plot A shows that the flow from the pipe 1 is interfered

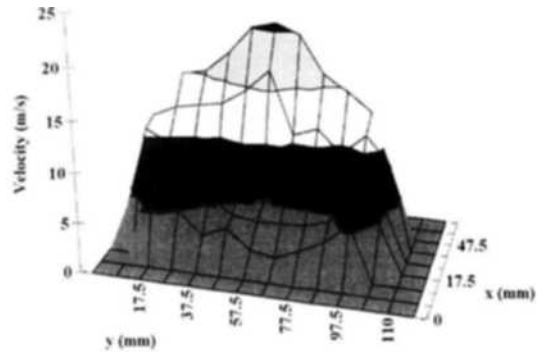


Fig. 19 Flow distribution in CCC under transient flow, 2500 rpm condition using LDV

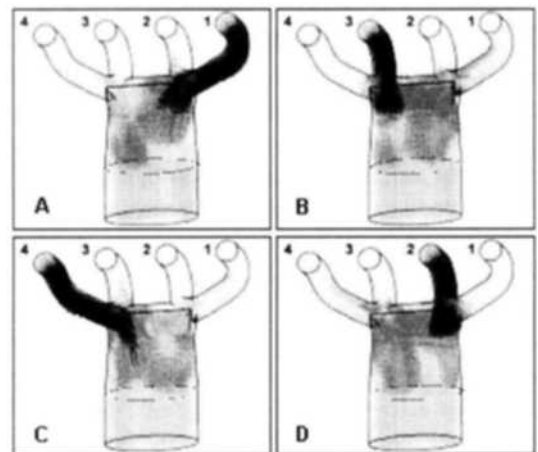


Fig. 20 Representative sequence of flow in exhaust manifold and CCC under transient condition using numerical analysis

by the earlier flow fields of the pipe 2 and 4, an increased flow resistance. On the plot B, the flow field of the pipe 3 is interfered by the earlier flow fields of the pipe 2 and 1. As a consequence, the flow expands more rapidly than in the steady flow conditions, yielding more uniform flow distribution. This might explain why the uniformity index is higher in transient conditions. The uniformity index determined from the CFD analysis was 0.93 for the transient condition.

5. Conclusions

Through the experiments and analysis of flow characteristics of CCC substrate, the following points are concluded :

- (1) The physically reasonable data was obtained through the CCC inlet velocity measurement by pitot tube, LDV and flow visualization.
- (2) The exhaust flow might concentrate on the particular region according to the shape of exhaust manifold.
- (3) In case of a transient condition, the sequential exhaust makes the flow distribution uniform. Therefore the exhaust manifold should be optimally designed when CCC is applied to exhaust system.
- (4) The results of numerical analysis coincide with experimental result very well ; therefore, an analytic method can be useful for the prediction of CCC flow distribution and optimization of CCC design.

References

Byung Hyouk Min, Jin Taek Chung, Ho

Young Kim and Simsoo Park, 2002, "Effects of Gas Composition on the Performance and Emissions of Compressed Natural Gas Engines," *KSME international journal*, Vol. 16, No. 2, pp. 219~226.

Cho, Y. S. et al., 2001, "A study of Measurement and Analysis of Flow Distribution in a Close-Coupled Catalytic Converter," *Transaction of KSME B*, Vol. 25, No. 4, pp. 533~539.

Cyeung Ho Choi, Sung Bin Han and Yun Joung Chung, 2003, "The effects of Hydrogen Enrichment on Exhaust Emissions and Thermal Efficiency in a LPG Fuelled Engine," *KSME international journal*, Vol. 17, No. 8, pp. 1196~1202.

Herman Weltens et al., 1993, "Optimisation of Catalytic Converter Gas Flow Distribution by CFD Prediction," *SAE 930780*.

Kim, M. H. et al., 1992, "A Study on the Flow Characteristics of the Catalytic Converter in Automotive Emission," *KSAE 923925*.

Lai, M. C. et al., 1991, "Three-dimensional Simulations of Automotive Catalytic Converter Internal Flow," *SAE 9100200*.

Manshik Kim and Kyoungdoug Min, 2001, "Calculation of Fuel Spray Impingement and Fuel Film Formation in an HSDI Diesel Engine," *KSME international journal*, Vol. 16, No. 3, pp. 376~385.

Star-CD Ver. 3.0 User's Manual, 1996, Computational Dynamics Limited.

Will, N. S. and Bennett, C. J., 1992, "Flow Maldistributions in Automotive Converter Canisters and Their Effect of Emission Control," *SAE 922339*.